

Additive Design Mimics the Strength and Architect of Nature

Muhannad Ahmed Obeidi^{1,2,3,*}

¹School of Mechanical and Manufacturing Engineering, Dublin City University, DCU, Ireland

²I-Forma Advanced Manufacturing and Research Centre, Ireland

³Advanced Processing Technology Centre APT, Ireland

Abstract: It is believed that the best parts' design and performance is that which mimics the creation of nature. Palm is a very good example of an extra ordinary tree which must attract the attention of engineers and designers. In contrast with other types of trees, palms have a vascular, jumble, and spongy tissue stem instead of a wooden one. This is the reason why palm trees can with stand strong hurricanes while trees cannot. The stem of a palm is composed of three main parts. Those are the main stem body, the central core, and the leaves growing from the central core in circular and axial patterns along the core. This natural combination tissues of different construction provides an extra-flexibility to the main stem, enhance the relative movement of these components, and as a result enables the palm to bend massively without any catastrophic fracture. This exceptional construction inspired the author to design and manufacture a part which mimics the most public tree at the home country. The model was additively manufactured from 316L, tested for bending with and without heat treatment, and compare with cast part of similar material and dimensions. The aim was always to achieve improved mechanical properties and performance of AM parts with complex geometry.

Keywords: Additive manufacturing, Laser powder bed fusion, 316L stainless steel, Bending testing, porosity, Scanning strategy.

INTRODUCTION

When compared to cast material, metal products that have been additively manufactured (AM) have poor mechanical characteristics [1-5]. Physical, chemical, and mechanical qualities fall under this category like the high porosity, ductility, and tensile strength. Examples of mechanical properties are elastic modulus, ductility, and ultimate tensile strength (*i.e.* surface quality, coloration, and dimensional accuracy). The association between this effect and the input processing parameters was examined in several research studies [6-10]. The localized and high thermal energy delivered in a very brief period of time (milli or micro-second) that is utilized to melt the metal powder is the main cause of the poor/low properties [11-14]. Extremely rapid cooling rates of up to 10^{12} K/s [15] will result from this. In an effort to lessen this impact, research is being done. For example, monitoring and controlling the amount of the laser input volumetric thermal energy by modulating the processing parameters to reduce the thermal gradient [16-19]. Other research work was focused on the post processing of AM parts like the annealing heat treatment for the thermal stresses release, controlled chemical phase formation, and the ductility improvement [20-23].

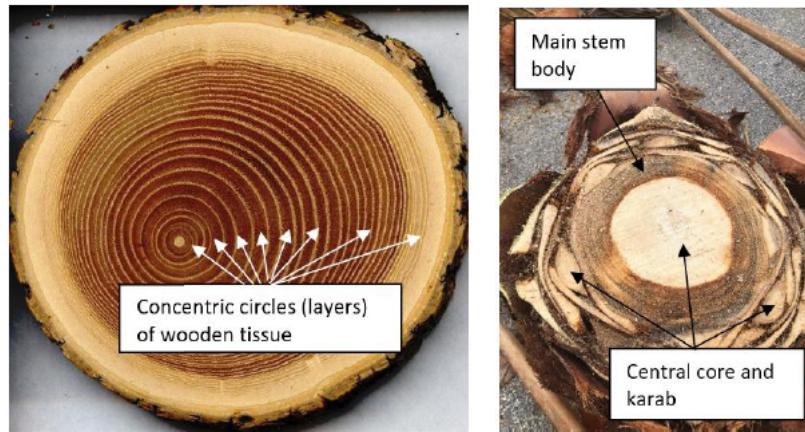
It is believed that significant and sophisticated designed engineering parts can always be inspired from nature around us. This was always showing robust success in designing interesting models in aviation, automotive, marine and submarine industry [24-26]. This study is focused on designing and manufacturing a mechanical part which can represent any metallic or non-metallic part exposed to bending load. The design reflects the exceptional and unique, external/internal construction of the palm which enables the tree to withstand sever weather conditions and hurricanes, Figure 1(c).

The apex of a palm tree has more than 50 mature leaves but only one stem and no branches. When the leaf first emerges from the stem body, it is relatively wide in the area where it grows. Typically, when trees develop, their leaves are removed. As opposed to the stem, the root portion of a leaf is known as the "Karab," and it is made up of denser tissue (a, and b). Compared to other wooden stem trees before they fractured, the many spongy and fiber tissues provide a flexible structure that is robust enough to resist and bend during the wind.

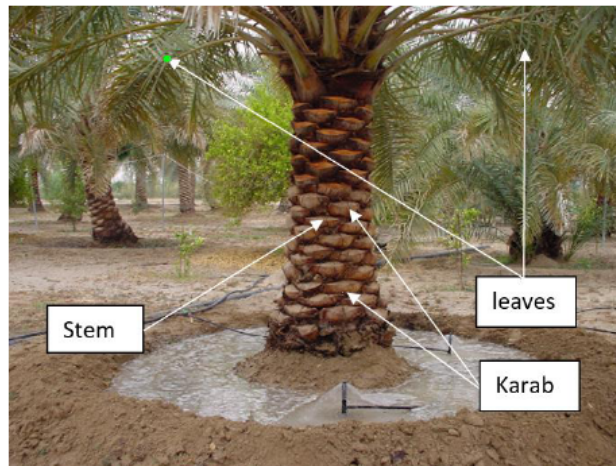
FABRICATION AND EXPERIMENTAL PROCEDURE

A laser-powder bed fusion (L-PBF) metal printer AconityMINI from Aachen, Germany was used to produce the metal samples used in this study. The 316L stainless steel powder used was gas atomised

*Address correspondence to this author at the School of Mechanical and Manufacturing Engineering, Dublin City University, DCU, Ireland; E-mail: muhannad.ahmedobeidi@dcu.ie



(a)



(b)



(c)

Figure 1: (a) a comparison between the stem cross-section of a tree and a palm, (b) the architecture of a palm tree, and (c).

with particle size distribution (PSD) of D_{10} : 15.5 μm , D_{50} : 30 μm , and D_{90} : 63 μm measured by using Malvern Mastersizer 3000. The chemical composition is listed in Table 1 as supplied by Carpenter Additive,

UK.

A cast sample of similar material was machined to the same dimensions of 10 mm diameter and 60 mm

Table 1: Chemical Composition of the 316L Stainless Steel in (wt%)

C	Cr	Cu	Mn	Mo	Ni	N	O	P	Si	S	Fe
0.03	17.6	0.02	0.66	2.38	12.5	0.09	0.03	0.007	0.65	0.006	Bal

length for comparison. The additively manufactured samples were designed in four different models. Two of these models were modified to mimic the internal construction of the palm tree which is mainly composed of two main parts, the main stem body and the central core. The latter itself is also composed of two parts; the central rod and the karab. The other two sets of samples were printed as solid cylinders. Each set of these samples were manufactured by using a unique scanning strategy and processing parameters. The scanning strategy and processing parameters were designed in two scenarios to produce (a) solid (high density) part and (b) pore (low density) part as explained below. The resulting Volumetric Energy Density (VED) was calculated as:

$$\text{VED (J/mm}^3\text{)} = \frac{\text{Laser beam power (W)}}{\text{Scanning speed (}\frac{\text{mm}}{\text{sec}}\text{)} \times \text{Laser spot size (mm)} \times \text{Hatch spacing (mm)}}$$

VED refers to the amount of thermal energy applied to the metal powder during the fusion process. It is a significant term which can be used efficiently to compare a characterised property of an AM part. A high VED level can lead to over-melting, keyhole formation and then high porosity while low value can result in lack of melting and parts may distorted during the printing process.

As can be seen, the (solid) part was printed with high laser beam power, low scanning speed and small hatch spacing allowing for the overlap of the consecutive laser beam tracks. This will result in a relatively higher input volumetric thermal energy compared to that of the pore scanning strategy and then more melting of the metal powder is applied. Additionally, the solid parts were produced by applying an angular rotation increment of 67° in each fused layer. In contrast, fixed scanning strategy with no laser

tracks rotation was applied during the fusion of the pore parts (see the video attached in the supplementary documents).

Moreover, two sets of palms were manufactured by alternating the pore and solid set of parameters on the (stem body) and the (core-karab) body. Another two sets were produced by using the solid set of processing parameters on one set and the pore on the other, see Figure 6. The produced samples were tested for bending in both as-built and after heat treatment conditions. Zwick 50 kN machine was used during the bending test with a test rate of 1 mm/min until fracture and a support span width adjusted to 40 mm. The testing machine is fitted with Zwick TestXpert software which records the force applied versus the deflection of the sample.

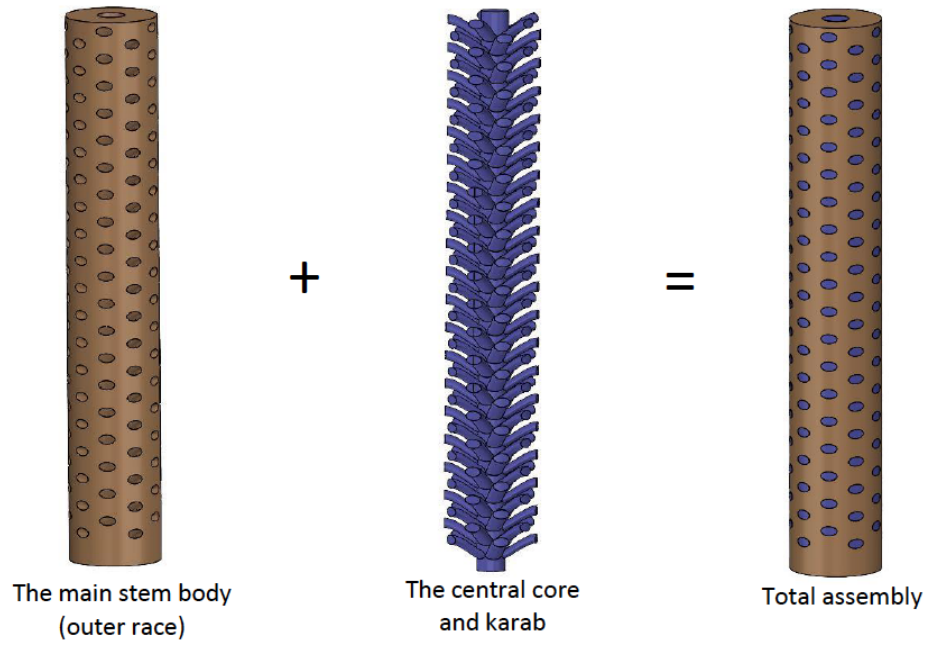
The heat treatment process was carried out by heating the samples up to 500 °C in an argon gas environment with heating rate of 10 °/min and holding for 1 hour followed by furnace cooling. The following Figure 2(a) shows the design of the two parts of the palm with their assembly and (b) shows a cross-sectional and magnified view of these parts.

Figure 3(a,b,c) shows the printing strategy from the Aconity Studio software for the (a) solid (stem)-pore (karab), (b) pore (stem)-solid (karab), and (c) shows the interfering contours of the stem-karab parts. A 100 microns contour (off-set) was always applied on the outside of the build part. This would results in 200 microns overlapping (OV) off-sets at the interface area shown in Figure 3 (right).

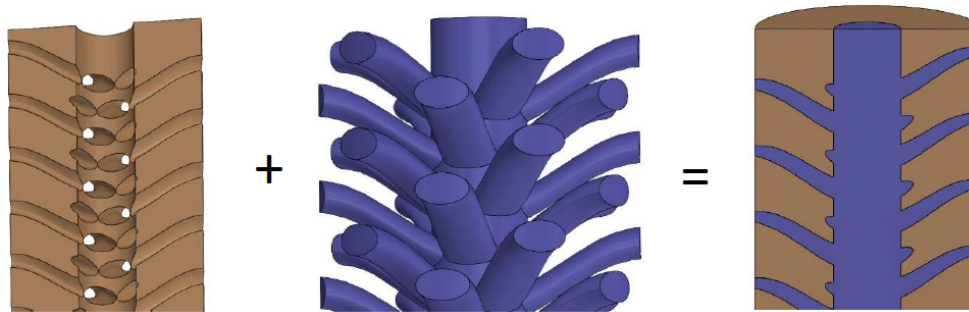
A better view of the build process can be found in the attached documented video.

Table 2: The Processing Parameters used During the Study

Microstructure Type	Laser power (W)	Scan speed (mm/sec)	Hatch space (µm)	Spot size (µm)	Layer thickness (µm)	VED (J/mm ³)
Solid	180	1000	50	70	40	51.4
Pore	140	1500	90	90	40	11.5



(a)



(b)

Figure 2: CAD design of the two main parts of the 316L palm and their assembly.

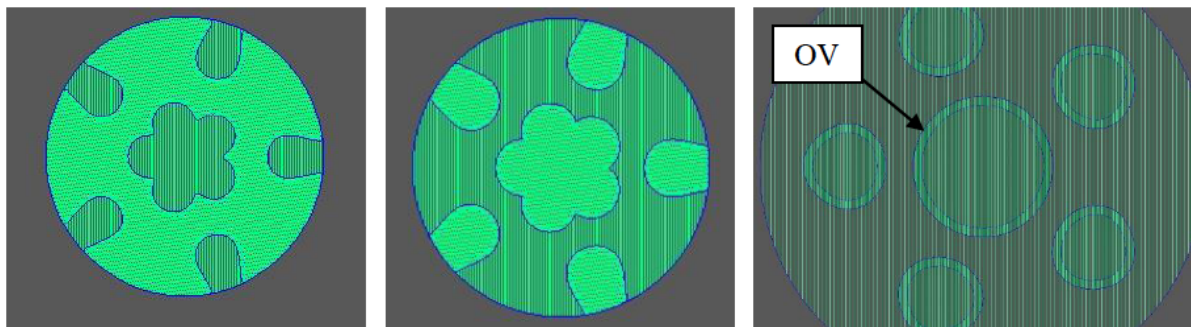


Figure 3: The scanning strategy for the build of a single layer as can be seen in Aconity Studio software. Solid stem-pore karab (left), pore stem-solid karab (middle), and overlapping contour (right).

The as-build and heat treated samples were tested for 3-points bending test as shown in Figure 4 below from the Zwick 50 testing machine.

RESULTS AND DISCUSSION

During the assessment and optimisation process, the extra pores microstructure was avoided in order to



Figure 4: The 3-Points bending experimental set up.

reduce the degradation in the mechanical strength of the produced beams. The following Figure 5 is an example of a beam produced with high porosity level due to the lack of melting. It can be seen in this figure that the overlapping contours off-set shows a significant melting and improved density caused by the remelting.

The optimised processing parameters employed in this study were selected based on results from the

literature, previous studies for the author, and a preliminary scanning test. The aim was always to produce part microstructures with distinguished densities. Those processing parameters are listed in Table 2.

The following Figure 6 shows the printed parts after removing from the AconityMINI metal printer. The parts were then removed from the build plate by using wire EDM machine.

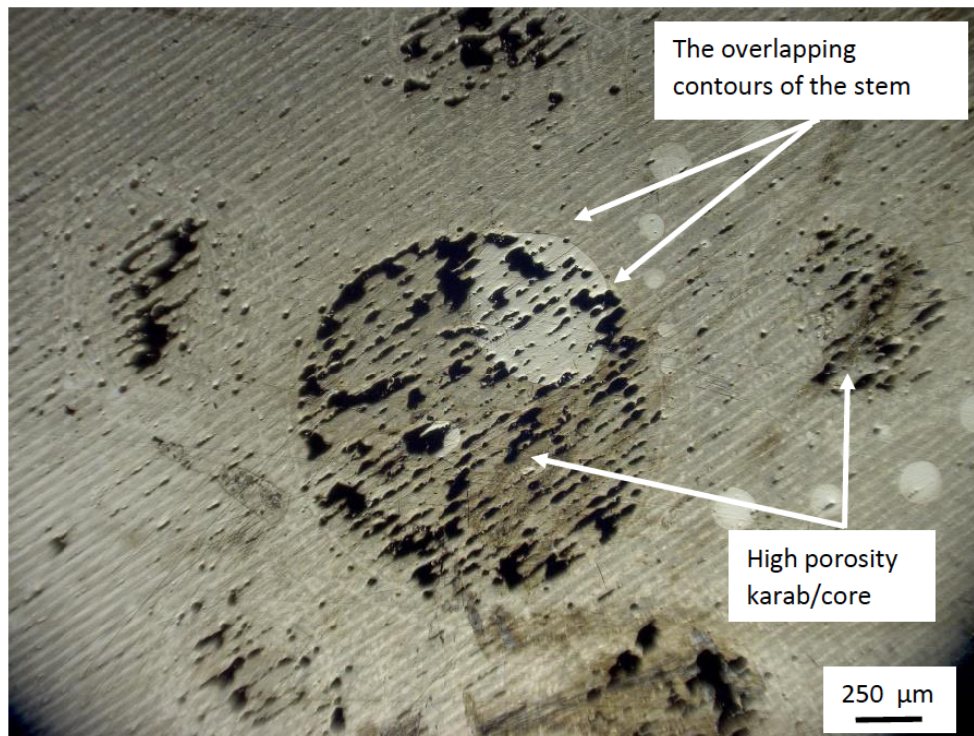


Figure 5: High porosity microstructure which is intentionally Produced on the karab/core portion on the beam sample.

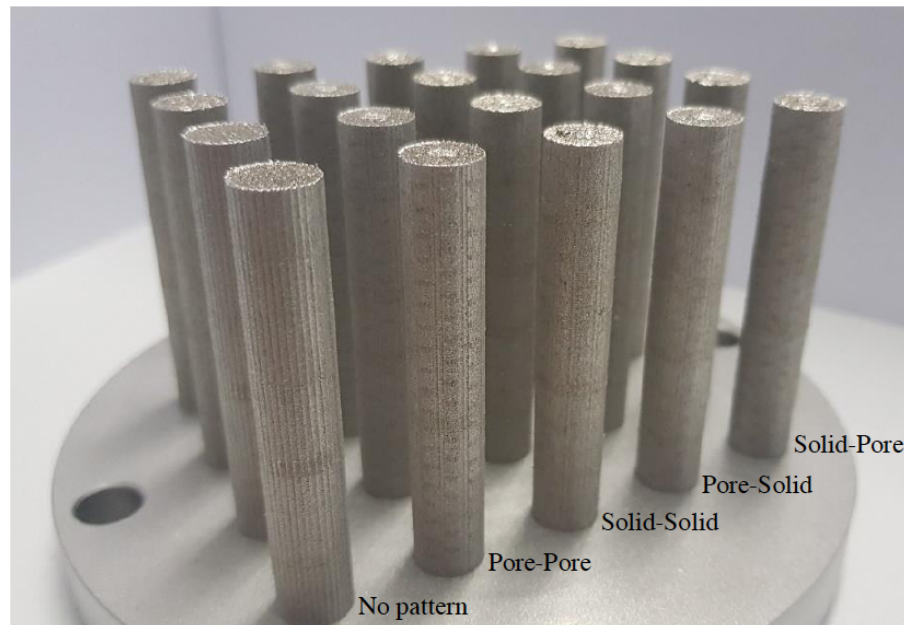


Figure 6: The produced samples after removal from the metal printer chamber.

The melt-pool temperature history during the entire build process was obtained by means of a pyrometer from KLEIBER Infrared GmbH. The pyrometer detects the light emitted from the melt-pool in the infra-red (IR) range of 1500 to 1700nm.

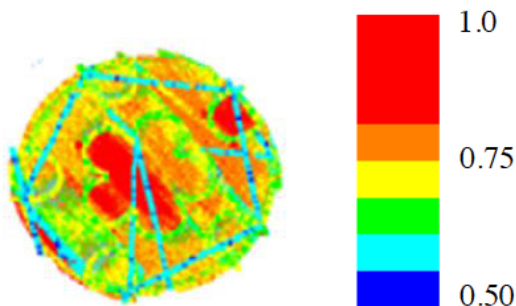


Figure 7: The live time melt-pool temperature profile as recorded by means of IR pyrometer.

The melt-pool temperature difference observed between the solid and pore parts melted in a single build layer was found to be approximately 50% on a normalised scale.

As a reference comparison, the cast material sample exhibited a yield point at a force of 7 kN and deflection of 1 mm. The tested samples showed a variant bending performance with reference to the scanning strategy and internal texture. Figure 8(a) below shows the bending plot for the cylindrical samples (no texture) printed in solid (sample no. 3) and

pore strategy (sample no. 4) without heat treatment and sample no. 1 and 2 after annealing. Similar to the results reported in the literature in testing AM parts for tension and compression [27, 28], the tested samples showed a clear reduction in the yield point and in the total deflection value compared to that of the cast material. This is an expected result for AM parts which agree well with the literature. Moreover, a noticeable enhancement in the yield point was noticed after heat treatment which can be explained by the precipitation, grain growth, and the more homogeneity in mechanical properties aiding the strength of the tested metal.

On the other hand, the textured samples printed with the stem-karab pattern exhibit significant improvement in the bending strength with a yield point of approximately equal or higher than the cast metal, Figure 8(b). This result was noted for both scenarios with and without heat treatment. Similar results were obtained during testing the (solid-solid) and (pore-pore) pattern cylinders indicating the compound effect of the cavities (grooves) in the stem and the karab on reinforcing the AM part. The curved geometry of the karab with the elliptic cross-sectional area and the normal distribution along and around the main axis of the core contribute in the bending stress distribution into multiple axes and circumferential components. In this figure, sample no. 7 was produced with pore stem and solid core/karab and sample no. 8 with solid stem and pore core/karab both without heat treatment.

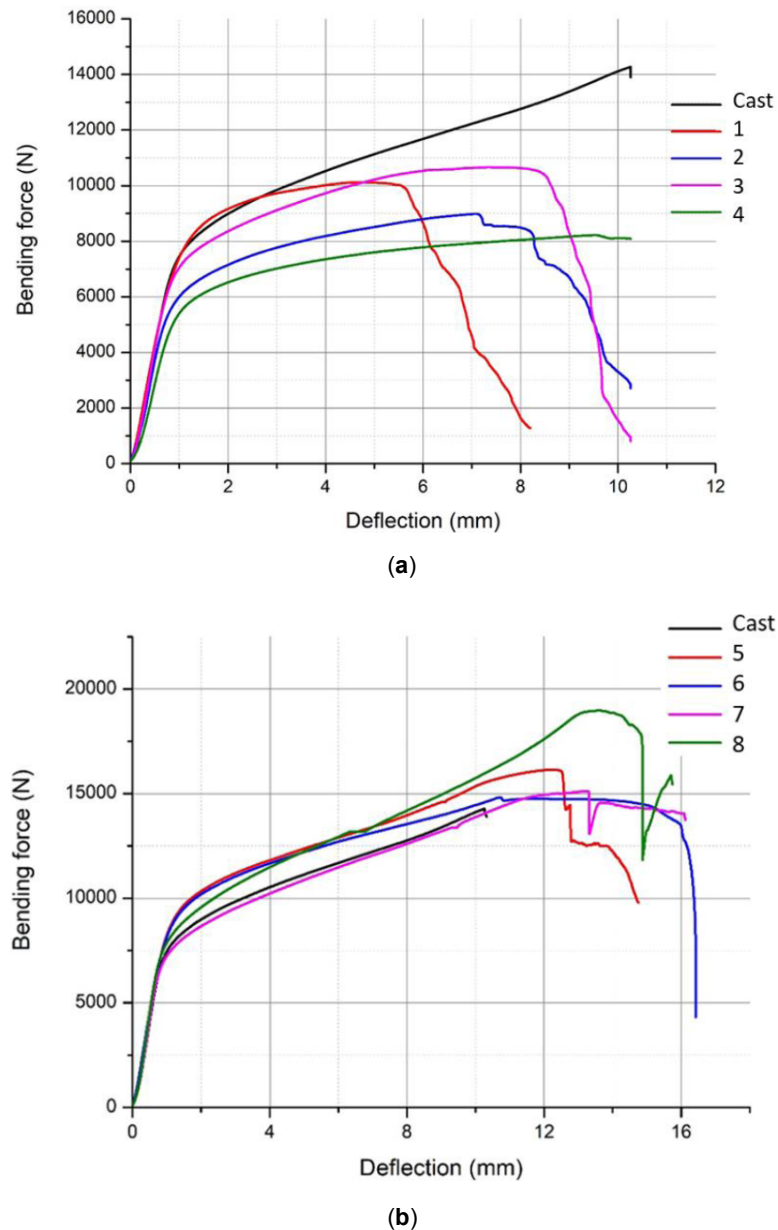


Figure 8: The bending test results of (a) AM cylinders, and (b) AM cylinder pattern assembly.

Samples no. 5 and 6 are the heat treated samples of the previous.

During the bending of cast and AM cylinders, it is known that a compression stress is created on the upper side of the cylinder while a tensile stress is created at the bottom, Figure 9(a). Also, a positive (clockwise) bending moment is created on the left of the exerted force and a negative (anticlockwise) is on the right side. The failure is most likely to be initiated at the bottom side when the tensile stress exceeds its maximum value.

In contrast, when the bending force is applied on the AM palm cylinder with reinforcing karab (green arrow in Figure 9(d)), a reaction force(s) will be resulted on the opposite end of each karab on the core axis. Also, the compression stress on the top surface pushes the karab always to the left (the pattern direction, blue arrows in Figure 9(d) while the stem material in between resist that. The reaction forces coming from the bottom of the karab versus the compression forces on the top generates individual negative moments on the top karab which reduces the positive (anticlockwise) moment and enhance the

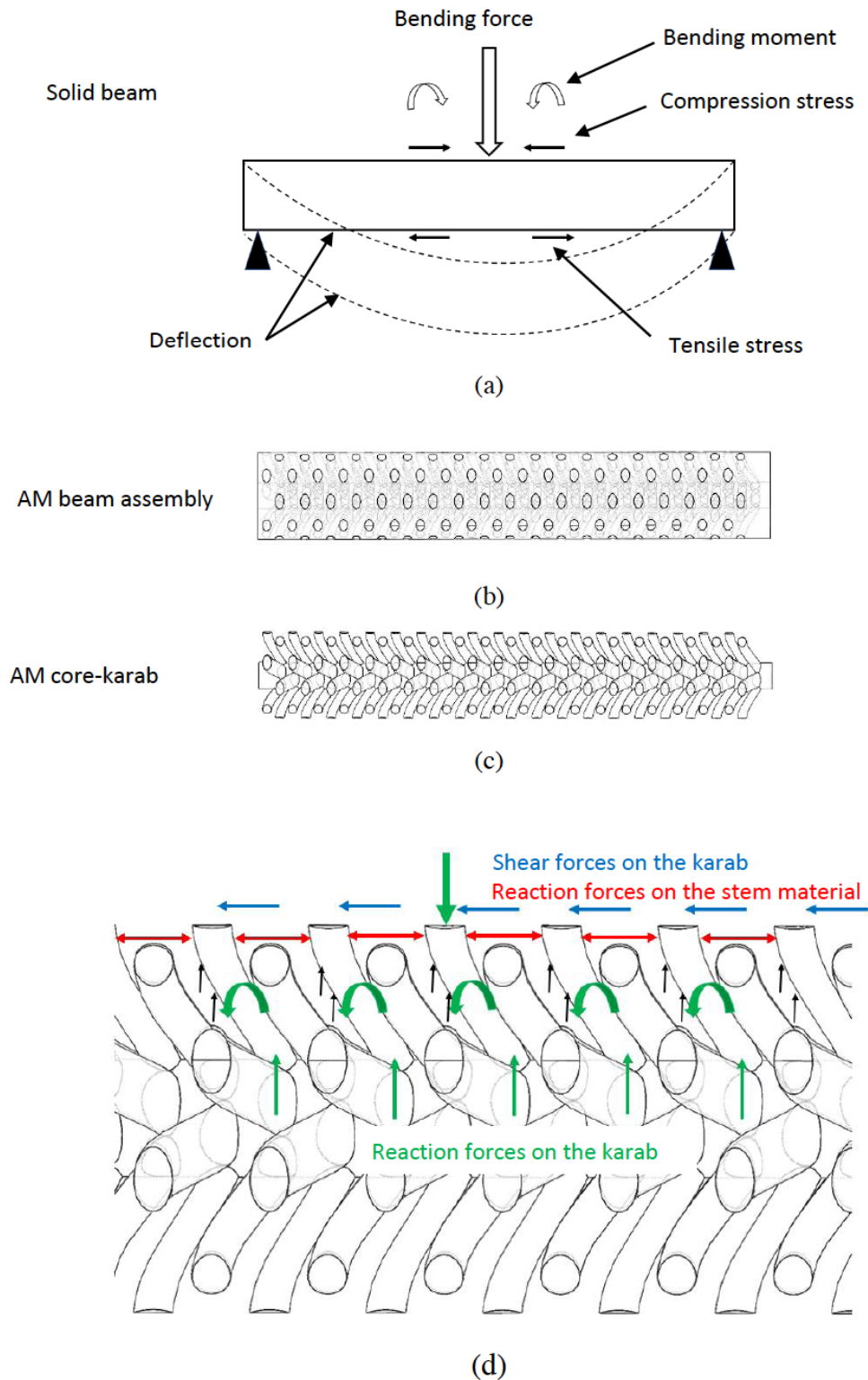


Figure 9: The bending of solid and AM cylinders.

bending strength. Moreover, the inclined orientation and the radial distribution pattern of the karab along the core, contribute massively in dissolving the forces and stress in multiple directions which are the main reason for the enhanced yield point.

Keyence optical microscope images below show the cross-sectional view of the AM beams. The images were obtained for both the as-built and heat treated samples. The melt-pool, laser tracks, and grain boundaries were clearly noted on the as-built samples

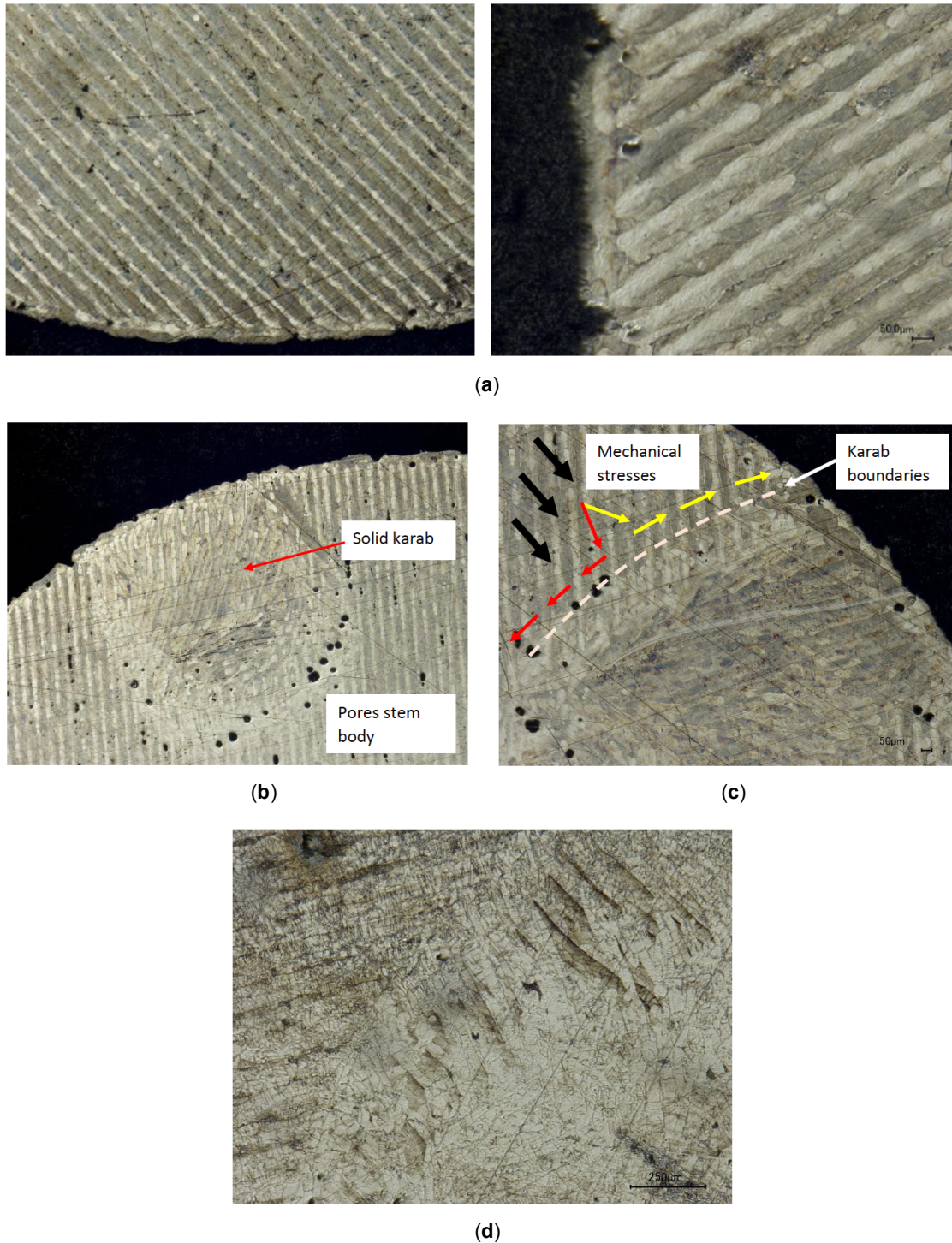


Figure 10: Optical microscope images (a) the stem body, (b) pore stem and solid karab, (c) bending and shear stresses reorientation around the karab rib, and (d) heat treated sample cross-section.

as opposed to the heat-treated samples (Figure 10 a, b, and c). This can be explained by the grain growth and interfere between the neighbouring boundaries.

CONCLUSION

Nature is always the optimum inspiration resource for smart, functional, and powerful designs. In this

study, an interesting design model was borrowed from the palm trees to solve one serious problem in additive manufacturing. The relative movement between the different tissue besides, the flexible and elastic shear occurring inside the palm, enable the tree to compensate the great deflection due to bending caused by hurricanes. This phenomena was used in

this study to prove the force of nature and to mitigate the reduced mechanical properties of an AM part. It was noted that the compound construction of an AM part (stem-karab) has a stronger effect than the scanning strategy (solid-pore) on the improved mechanical properties. By employing such thinking and design, engineered parts with complex geometries and/or special metal type which are difficult to be machined, it is now possible to achieve the cast material properties like stiffness, yield point and ductility. The study suggests and encourages the use of this design and other naturally created constructions and geometries to solve serious problems in aerospace, automotive, and biomedical industries and produce parts of high performance, less weight, cost and material involved.

ACKNOWLEDGMENTS

This publication has emanated from research supported by a research grant from Science Foundation Ireland (SFI) under grant number 16/RC/3872 and is co-funded under the European Regional Development Fund.

REFERENCES

- [1] Moghaddam N.S, *et al.* Achieving superelasticity in additively manufactured NiTi in compression without post-process heat treatment. Scientific Report, www.nature.com/scientificreports, (2019).
- [2] Moghaddam, N. S. *et al.* Metals for bone implants: Safety, design, and efficacy. *Biomanufacturing Reviews* 2016; 1: 1. <https://doi.org/10.1007/s40898-016-0001-2>
- [3] Bansiddhi, A., Sargeant, T., Stupp, S. & Dunand, D. Porous NiTi for bone implants: a review. *Acta biomaterialia* 2008; 4: 773-782. <https://doi.org/10.1016/j.actbio.2008.02.009>
- [4] Obeidi M. A., "Metal additive manufacturing by laser-powder bed fusion: Guidelines for process optimisation", *Results in Engineering*, 2022; 15: 100473. <https://doi.org/10.1016/j.rineng.2022.100473>
- [5] Shabalovskaya, S. A. Surface, corrosion and biocompatibility aspects of Nitinol as an implant material. *Bio-medical materials and engineering* 2002; 12: 69-109.
- [6] Moghaddam, N. S. *et al.* In Behavior and Mechanics of Multifunctional Materials and Composites XII. 105960H (International Society for Optics and Photonics).
- [7] Ibrahim, H. *et al.* In Vitro Corrosion Assessment of Additively Manufactured Porous NiTi Structures for Bone Fixation Applications. *Metals* 2018; 8: 164. <https://doi.org/10.3390/met8030164>
- [8] Ma, C. *et al.* improving surface finish and wear resistance of additive manufactured nickel-titanium by ultrasonic nano-crystal surface modification. *Journal of Materials Processing Technology* 2017; 249: 433-440. <https://doi.org/10.1016/j.jmatprotec.2017.06.038>
- [9] Obeidi M. A., *et al.*, Laser beam powder bed fusion of nitinol shape memory alloy (SMA). *Journal Of Materials Research And Technology*; 2021; 14: 2554-2570. <https://doi.org/10.1016/j.jmrt.2021.07.126>
- [10] Obeidi M. A. *et al.* Achieving high quality nitinol parts with minimised input thermal energy by optimised pulse wave laser powder bed fusion process. *Results in Materials* 14 100279, (2022). <https://doi.org/10.1016/j.rinma.2022.100279>
- [11] Zhao, *et al.* A 3D dynamic analysis of thermal behaviour during single-pass multi-layer weld-based rapid prototyping. *J. Mater. Process. Technol* 2011; 211(3): 488-495. <https://doi.org/10.1016/j.jmatprotec.2010.11.002>
- [12] Chen X., *et al.* Microstructure and mechanical properties of the austenitic stainless steel 316 L fabricated by gas metal arc additive manufacturing. *Mater. Sci. Eng. A* (2017) <https://doi.org/10.1016/j.msea.2017.05.024>
- [13] Fachinotti Vc.D, *et al.* Finite-element modelling of heat transfer in shaped metal deposition and experimental validation *Acta Mater.*, 2012; 60: 6621-6630 <https://doi.org/10.1016/j.actamat.2012.08.031>
- [14] Chen X., *et al.* Effect of heat treatment on microstructure, mechanical and corrosion properties of austenitic stainless steel 316L using arc additive manufacturing. *Materials Science and Engineering: A*, (2018). <https://doi.org/10.1016/j.msea.2017.10.002>
- [15] J. Dutta Majumdar, I. Manna, *Laser processing of materials*, Sadhana. 2003; 28: 495-562. <https://doi.org/10.1007/BF02706446>
- [16] Guo Q., *et al.* In-situ characterization and quantification of melt pool variation under constant input energy density in laser powder bed fusion additive manufacturing process. *Additive Manufacturing*, (2019). <https://doi.org/10.1016/j.addma.2019.04.021>
- [17] Farshidianfar M., *et al.* Effect of real-time cooling rate on microstructure in Laser Additive Manufacturing *J. Mater. Process. Technol.*, 2016; 231: 468-478. <https://doi.org/10.1016/j.jmatprotec.2016.01.017>
- [18] Campanelli S., *et al.* Analysis of the molten/solidified zone in selective laser melted parts SPIE LASE., 8963, Article 896311. (2014) <https://doi.org/10.1117/12.2042170>
- [19] Nelson J. *Selective Laser Sintering: a Definition of the Process and an Empirical Sintering Model* Ph.D. thesis, University of Texas at Austin, Austin, TX (1993)
- [20] Schwind M., *et al.*, σ -phase precipitation in stabilized austenitic stainless steels, *Acta Mater.* 2000; 48(10): 2473-2481. [https://doi.org/10.1016/S1359-6454\(00\)00069-0](https://doi.org/10.1016/S1359-6454(00)00069-0)
- [21] Olson D., Prediction of austenitic weld metal microstructure and properties, *Weld. J.* 1985; 281-295.
- [22] Lippold J. *et al.* Solidification of austenitic stainless steel weldments Part III-the effect of solidification behavior on hot cracking susceptibility, *Weld. J.* 388-396 (1982) G.B. Senay, *et al.*, Prediction of σ phase precipitation in type 316FR stainless steel weld metal, *J. Jpn. Weld. Soc.* 2013; 31(4): 168s-172s. <https://doi.org/10.2207/qjwjs.31.168s>
- [23] Okabayashi H., Mathematical approach to σ phase precipitation in austenitic stainless steel welds, *Mater. Trans.* 37 (5) 970-974. (1996) <https://doi.org/10.2320/matertrans1989.37.970>
- [24] Young, J., "numerical simulation of the unsteady aerodynamics of flapping airfoils", Ph.D. thesis, The University of New South Wales, (2005).
- [25] Joshua Ott *et al.*, "Algorithmic-driven design of shark denticle bioinspired structures for superior aerodynamic properties", *Bioinspiration & Biomimetics*, (2020).
- [26] Brucher, R., Rydill, L., "Concepts in submarine design", Cambridge Ocean Technology, Series 2, Department of Mechanical Engineering, University College London, ISBN 0521416817, (1999)

- [27] Collins PC, Brice DA, Samimi P, Ghamarian I, Fraser HL. "Microstructural control of additively manufactured metallic materials. *Annu Rev Mater Res* 2016; 46: 63e91. <https://doi.org/10.1146/annurev-matsci-070115-031816>
- [28] Ahmed Obeidi, M., *et al.* "Comparison of the porosity and mechanical performance of 316L stainless steel manufactured on different laser powder bed fusion metal additive manufacturing machines", *Journal of Materials Research and Technology*, (2021). <https://doi.org/10.1016/j.jmrt.2021.06.027>

Received on 02-02-2023

Accepted on 28-02-2023

Published on 02-03-2023

DOI: <https://doi.org/10.31875/2410-4701.2023.10.01>

© 2023 Muhannad Ahmed Obeidi; Zeal Press.

This is an open access article licensed under the terms of the Creative Commons Attribution License (<http://creativecommons.org/licenses/by/4.0/>) which permits unrestricted use, distribution and reproduction in any medium, provided the work is properly cited.